

A Vector Intermodulation Analyzer Applied to Behavioral Modeling of Nonlinear Amplifiers With Memory

Aaron Walker, *Member, IEEE*, Michael Steer, *Fellow, IEEE*, and Kevin G. Gard, *Member, IEEE*

Abstract—A large signal vector intermodulation network analyzer with a dynamic range of 90 dB and phase resolution of better than 2° is reported. The analyzer is used in conjunction with a multislice behavioral model to characterize memory effects in three different RF power amplifiers: an MOSFET instrumentation amplifier, a multistage GaAs/silicon-based broadband microwave integrated-circuit amplifier, and an SiGe HBT monolithic-microwave integrated-circuit amplifier. The multislice behavioral model architecture builds on conventional single-tone AM-AM and AM-PM modeling extended to capture long-term memory effects that are characterized by asymmetric intermodulation distortion (IMD). Phase asymmetries of upper and lower IMD are captured. A systematic procedure for extracting the model is presented.

Index Terms—Behavioral modeling, intermodulation asymmetry, intermodulation phase measurement, multislice model, nonlinear memory effects.

I. INTRODUCTION

A BEHAVIORAL model of an RF front-end enables system-level performance (such as bit error rate and spectral regrowth) to be determined at the circuit-design or system-integration stages. The models themselves can be extracted from external-terminal characterizations of subsystem components using discrete-tone signals. Traditionally such models are based on single-tone measurements with the input swept over power and the amplitude and phase responses measured experimentally or in a circuit simulation. With linear transfer functions, these models can capture some memory effects manifesting themselves as RF frequency-dependent characteristics. However, the models do not capture long-term memory effects. These effects result in large part from the interaction of down-converted signals with baseband circuitry, long-term trapping, and thermal transients. Capturing long-term memory effects is essential with digitally modulated systems as spectral regrowth and in-band and out-of-band intermodulation levels must be kept very low. Here, we present a comprehensive approach for characterizing the amplitude and phase of intermodulation distortion (IMD) using a vector intermodulation analyzer (VIMA); a multislice behavioral model architecture

(the multislice model) that captures long-term memory effects; and a procedure for extracting the model from measurements. The multislice model captures amplitude and phase asymmetries of the intermodulation response of RF circuits.

RF nonlinear behavioral models attempt to capture complex behavior from simple measurements, especially using discrete tones [1]–[5]. Intermodulation-distortion asymmetries and memory effects (both macrolevel wideband and microlevel narrowband or modulation bandwidth-dependent effects) comprise the core of the complexities that may arise in an RF or microwave communication system [6]–[8]. Experimental techniques employing stimulus similar to that used in digitally modulated communications systems have also been developed [2], [3].

The main contribution of this study is the development of a multislice model to track the amplitude and phase responses of a nonlinear system under multitone stimulus using relatively few laboratory measurements. This paper describes enhancements of a previously reported intermodulation measurement system [10], [11], but now with higher dynamic range and relative phase determination. A review of the existing systems for measuring the phase of either harmonics or discrete tone intermodulation products is also presented in [10]. Three RF power amplifiers with various nonlinear characteristics are considered, which are: 1) a MOSFET instrumentation amplifier; 2) a GaAs-based broadband microwave integrated-circuit (MIC) amplifier; and 3) an SiGe HBT monolithic-microwave integrated-circuit (MMIC) amplifier. The results of performing the intermodulation phase measurement on these amplifiers demonstrates the effectiveness of the model architecture and extraction procedure for capturing the effect of multiple nonlinear processes. In [11], a multislice behavioral model was shown to model the phase nonlinearities that are evident in the intermodulation product. This model is developed for each of the amplifiers considered here.

II. VIMA

The VIMA uses a bridge technique and three phase-locked sources (see Fig. 1) [10]. The phase-locked sources maintain phase coherence, whereas alternative frequency-locked sources (the most common) do not. In a typical measurement, Sources 1 and 2 generate the two-tone test signal and the third source generates a signal corresponding to either the lower or upper intermodulation signal. The third tone, however, could be set to be one of the original tones, an harmonic, or any other intermodulation tone. The system is based on cancellation of the

Manuscript received January 2, 2006.

A. Walker was with the Department of Electrical and Computer Engineering North Carolina State University, Raleigh, NC 27695-7914 USA. He is now with Vadum Inc., Raleigh, NC 27613 USA (e-mail: aaron.walker@vaduminc.com).

M. Steer and K. G. Gard are with the Department of Electrical and Computer Engineering North Carolina State University, Raleigh, NC 27695-7914 USA.

Digital Object Identifier 10.1109/TMTT.2006.872810

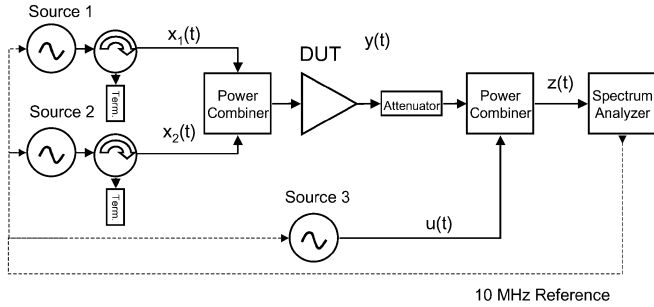


Fig. 1. VIMA incorporating phase-locked signal sources.

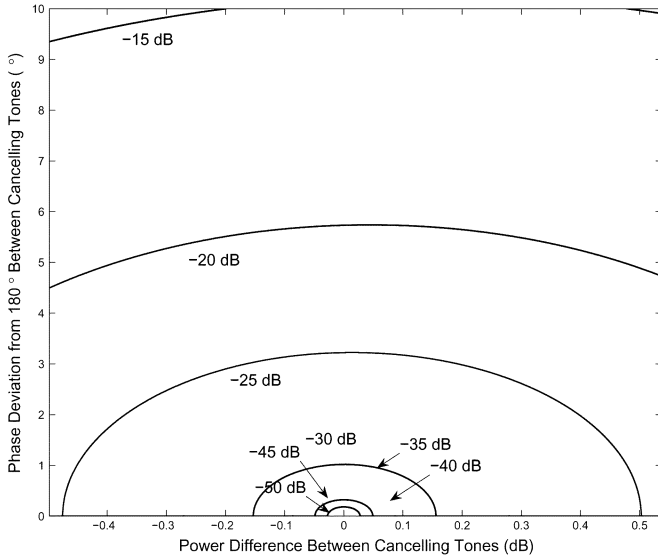


Fig. 2. Contour plot of magnitude of summation between two sinusoidal tones with the same frequency for amplitude and phase differences.

nonlinear spectral output products with a synthesizer to determine the phase as opposed to a reference nonlinear device commonly used in other systems (e.g., [12] and [13]). The phase captured by the measurement is relative, but is not arbitrary, and the phase reference of the IMD products can be determined by using single-tone AM-PM data. In particular, the definition of relative phase in this context is the same as that used by Suematsu *et al.* [12], where the phase reference is the phase measured in the small-signal regime in a one-tone test.

The VIMA (Fig. 1) has a large dynamic range enabling the system to measure the intermodulation product phase and magnitude for weak nonlinearities or small signals. A bridge technique, implemented by the power combiner, is used to compare the amplitude and phase of a distortion tone from the device-under-test (DUT) to the signal generated by a third signal source. In this bridge cancellation scheme, dynamic range determines the phase measurement uncertainty, as well as the uncertainty in the amplitude measurement. The phase uncertainty is computed based on the rejection equation for the summation of two sinusoidal tones at the same frequency. Fig. 2 presents the phase uncertainty as a contour plot (the error in the phase of opposing tones) versus the difference in power of the cancelling tones. The amplitude uncertainty is determined by the dynamic range of the spectrum analyzer, which corresponds to a system

TABLE I
DYNAMIC RANGE AND PHASE UNCERTAINTY/ERROR PERFORMANCE OF PUBLISHED IMD PHASE MEASUREMENT SYSTEMS

Group	Year	Dynamic Range (dB)	Phase error
Suematsu, et al. [12]	1997	35 [†]	$< \pm 2^\circ$
Yang, et al. [13]	2001	unknown	$> \pm 1.8^\circ$
Maury NVNA [15], [16]	2003-4	60	$< 3^\circ$
Vuolevi, et al. [17]	2001	40 [†]	$\pm 1.8^\circ$
Heymann, et al. [18]	2001	55	$\pm 10^\circ$
Crespo-Cadenas, et al. [19]	2005	60	$< 6^\circ$ [†]
Pedro, et al. [20]	2005	60 [†]	unknown
Walker, et al. [10]	2005	90	2° max., 0.5° avg.

[†] indicates estimated performance based on published results.

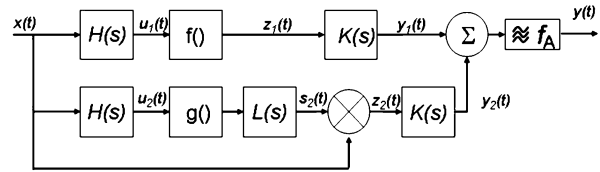


Fig. 3. Block diagram of the multislice behavioral model.

dynamic range of 90 dB and a maximum phase uncertainty of 2°. These are compared to reported schemes for measuring the amplitude and phase distortion in Table I.

The dynamic range of this system was determined by both measurement and inspection of the spectrum analyzer specifications [14]. The dynamic range is important at the weakest nonlinear response for the DUT. At low input power levels, the distortion in the analyzer front-end can overwhelm the DUT response. In this system, the stimulus power at the internal mixer was -40 dBm, while the weakest nonlinear device studied produced distortion products of -102 dBm at the mixer. During phase measurement, 30 dB of cancellation of the third-order intermodulation (IM3) tones was achieved, thus the dynamic range of the system was at least 90 dB. The analyzer specification lists the dynamic range as ~ 105 dB for a -40 -dBm power level, which verifies the observed measurements.

III. MULTISLICE BEHAVIORAL MODEL

Many microwave subsystems, e.g., amplifiers, have filtering or matching networks at their inputs and outputs so that only signals in the operating frequency band can be directly observed. The multislice model, shown in Fig. 3 for two slices, was introduced [8] to facilitate behavioral modeling using partially observed (in this case, band-limited) data. The model builds on conventional one-tone modeling practices as the first slice is derived from convenient AM-AM and AM-PM measurements. The second slice was initially added to reproduce amplitude asymmetries present in the IM3 products of an amplifier. The development is extended in the following sections to capture phase asymmetries as well. Additional slices can be added to the model to describe higher order effects that cannot be captured by one- and two-tone tests.

A. Analysis of First Slice

The multislice model is an architecture and each slice can be modeled by nearly any behavioral modeling technique. Here,

we use a Weiner–Hammerstein linear–nonlinear–linear (LNL) block model for the first slice. The nonlinearity $f(\cdot)$ is taken as a memoryless odd-ordered polynomial. The linear networks $H(s)$ and $K(s)$ capture frequency selectivity resulting, for example, from filters, matching networks, and reactive parasitics. The networks capture the macrolevel memory effect, which causes variations in the magnitude and phase response of the output as a function of the frequency of the input signal.

Given a general stimulus composed of Q incommensurate sinusoids,

$$x(t) = \frac{1}{2} \sum_{\substack{q=-Q \\ q \neq 0}}^Q A_q e^{j(\omega_q t + \phi_q)} \quad (1)$$

with $A_q = A_{-q}$, $\omega_q = -\omega_{-q}$ and $\phi_q = -\phi_{-q}$, the output of the linear network $H(s)$ is

$$u_1(t) = \frac{1}{2} \sum_{q=-Q}^Q A_q e^{j(\omega_q t + \phi_q)} |H(\omega_q)| e^{j(\phi_{H(\omega_q)})}. \quad (2)$$

After passing through the complex polynomial block, the output $z_1(t)$ for a given order n of the polynomial is given by

$$z_{1,n}(t) = \left\{ \frac{1}{2} \sum_{q=-Q}^Q A_q e^{j(\omega_q t + \phi_q)} |H(\omega_q)| e^{j(\phi_{H(\omega_q)})} \right\}^n \times |a_n| e^{j\phi_{a_n}} \quad (3)$$

with $z_1(t) = \sum_{n=0}^N z_{1,n}(t)$. The term ϕ_{a_n} is applied as a complex conjugate phase shift depending on the sign of the frequencies produced by raising the complex exponential representation to the power n .

The output of the first slice is

$$y_{1,n}(t) = |a_n| |K(\omega)| e^{j(\phi_{a_n} + \phi_{K(\omega)})} \times \left\{ \frac{1}{2} \sum_{q=-Q}^Q A_q e^{j(\omega_q t + \phi_q)} |H(\omega_q)| e^{j(\phi_{H(\omega_q)})} \right\}^n \quad (4)$$

where again the sign of $\phi_{K(\omega)}$ for a given expansion results in the production of a real overall result. The complete output of the first slice is given by $y_1(t) = \sum_{n=0}^N y_{1,n}(t)$. Expansion of (4) for a single order n yields

$$y_{1,n}(t) = |a_n| |K(\omega)| e^{j(\phi_{a_n} + \phi_{K(\omega)})} \times \frac{1}{2^n} \sum_{q_1=-Q}^Q \cdots \sum_{q_n=-Q}^Q A_{q_1} \cdots \times A_{q_n} |H(\omega_{q_1})| \cdots |H(\omega_{q_n})| \times e^{j(\Phi_{q_1} + \cdots + \Phi_{q_n} + \phi_{H(\omega_{q_1})} + \cdots + \phi_{H(\omega_{q_n})})}$$

where $\Phi_{q_i} = \omega_{q_i} t + \phi_{q_i}$ is a function of the frequency and initial phase of the individual tones. Using the concept of the frequency-mixing vector \vec{m} developed by Weiner and Spina [21], the output of (5) at a specific frequency can be determined. The mixing vector has $2Q$ entries and enumerates the collection of positive and negative frequencies in the desired product as $\vec{m} = [m_{\omega_{-Q}}, m_{\omega_{-Q+1}}, \dots, m_{\omega_1}, \dots, m_{\omega_Q}]$ with the constraint that $\sum_{q=-Q}^Q m_{\omega_q} = n$ for a given order. Using this convention, the output for a given \vec{m} is

$$y_{1,n,\vec{m}}(t) = \frac{|a_n|}{2^{n-1}} |K(\omega_{\vec{m}})| c_{\vec{m},n} A_{q_1} \cdots A_{q_n} |H(\omega_{\vec{m}})|^n \times \cos(\omega_{\vec{m}} t + \phi_{\vec{m}} + \phi_{H(\omega_{\vec{m}})} + \phi_{K(\omega_{\vec{m}})} + \phi_{a_n}) \quad (5)$$

with $\phi_{H(\omega_{\vec{m}})} = \sum_{\vec{m}} \phi_{H(\omega_{\vec{m}})}$. The coefficient $c_{\vec{m},n}$ is the multinomial expansion coefficient for the sum of permutations of $q_1 - q_n$ that generates \vec{m} . The multinomial is defined by

$$c_{\vec{m},n} = \binom{n}{\vec{m}} = \frac{n!}{m_{\omega_{-Q}}! m_{\omega_{-Q+1}}! \cdots m_{\omega_{Q-1}}! m_{\omega_Q}!}. \quad (6)$$

For a low number of tones, it is convenient to sum over all of the vectors \vec{m} that produce a specific frequency output for a polynomial of order N , as in [3]. The fundamental response of the first slice under a single-tone stimulus is then given by

$$y_{1,\vec{m}}(t) = \sum_{n=1}^N \frac{|a_n|}{2^{n-1}} \left(\frac{n-1}{2}, \frac{n+1}{2} \right) \times A_{\omega_1}^n |H(\omega_{\vec{m}})|^n |K(\omega_{\vec{m}})| \times \cos(\omega_{\vec{m}} t + \phi_{\omega_{\vec{m}}} + \phi_{H(\omega_{\vec{m}})} + \phi_{K(\omega_{\vec{m}})} + \phi_{a_n}). \quad (7)$$

The IM3 response predicted by the first slice with two-tone stimulus is

$$y_{1,\vec{m}}(t) = \sum_{n=3}^N \sum_{l=0}^{\frac{n-3}{2}} \frac{|a_n|}{2^{n-1}} \left(\frac{n-3}{2} - l, l, l+1, \frac{n+1}{2} - l \right) \times A_{\omega_1}^{2l+1} A_{\omega_2}^{n-2l-1} |H(\omega_{\vec{m}})|^n |K(\omega_{\vec{m}})| \times \cos(\omega_{\vec{m}} t + \phi_{\omega_{\vec{m}}} + \phi_{H(\omega_{\vec{m}})} + \phi_{K(\omega_{\vec{m}})} + \phi_{a_n}). \quad (8)$$

Expression (8) is identical for the upper and lower IM3 (IM3L) products. Thus, the well-known result from (8) is that a complex polynomial representation of a memoryless nonlinearity cannot produce IM3 products that have asymmetric amplitude or phase responses. Clearly the phase shift introduced by the polynomial coefficient is constant and shifts both IM3 products by the same amount.

Since a single complex polynomial cannot contribute to asymmetric behavior, an additional model component must be added. The multislice model seeks to employ slices that represent intuitive and realistic behavior, thus another slice

representing baseband upconversion effects that contributes to asymmetry will be considered.

B. Analysis of the Second Slice

The second slice shown in Fig. 3 is composed of identical linear networks for the macrolevel memory effects as the first slice, as well as an even-ordered complex polynomial ($g(x) = k_0 + k_2x^2 + k_4x^4 + \dots$) representing the nonlinearity, which generates the baseband terms. The linear network $L(s)$ consists of a real linear network with a low-pass response, which limits the components that get upconverted via the ideal mixer to the intermodulation products in the operating frequency band. The physical support of a baseband contribution results from several processes including cascade nonlinear effects due to input and output nonlinearities in bipolar junction transistor (BJT) devices and feedback of low-frequency distortion products through the dc-bias networks of an amplifier discussed in [6] and [17]. We will show here how the second slice reproduces this behavior and how the baseband component of the nonlinear response potentially leads to amplitude and phase asymmetries of the IM3 products.

The response of the second slice is similar to that of the first with the expression for $s_2(t)$ being equivalent to $y_1(t)$ or

$$s_{2,n}(t) = |k_n| |L(\omega)| e^{j(\phi_{k_n} + \phi_{L(\omega)})} \frac{1}{2^n} \times \sum_{q_1=-Q}^Q \dots \sum_{q_n=-Q}^Q A_{q_1} \dots A_{q_n} |H(\omega_{q_1})| \dots |H(\omega_{q_n})| \times e^{j(\Phi_{q_1} + \dots + \Phi_{q_n} + \phi_{H(\omega_{q_1})} + \dots + \phi_{H(\omega_{q_n})})}. \quad (9)$$

Now with $L(s)$ having a low-pass response with a cutoff frequency far lower than the stimulus frequencies, all harmonics of the even-order nonlinearity will be rejected. Taking the output $s_2(t)$ at the baseband component at $\omega_1 - \omega_2$, ($\omega_2 > \omega_1$) yields

$$s_{2,\omega_{\text{BBL}}}(t) = \sum_{n=2}^N \sum_{l=0}^{\frac{n-2}{2}} \frac{|k_n|}{2^{n-1}} \binom{n}{\frac{n}{2} - l, l, l+1, \frac{n-2}{2} - l} \times A_{\omega_1}^{2l+1} A_{\omega_2}^{n-2l-1} |H(\omega)|^n \times \cos(\omega_{\text{BBL}}t + \phi_{\text{BBL}} + \phi_{L(\omega_{\text{BBL}})} - \phi_{k_n}). \quad (10a)$$

Similarly, for $\omega_2 - \omega_1$,

$$s_{2,\omega_{\text{BBH}}}(t) = \sum_{n=2}^N \sum_{l=0}^{\frac{n-2}{2}} \frac{|k_n|}{2^{n-1}} \binom{n}{l, \frac{n}{2} - l, \frac{n-2}{2} - l, l+1} \times A_{\omega_2}^{2l+1} A_{\omega_1}^{n-2l-1} |H(\omega)|^n \times \cos(\omega_{\text{BBH}}t + \phi_{\text{BBH}} + \phi_{L(\omega_{\text{BBH}})} + \phi_{k_n}). \quad (10b)$$

assuming that $\phi_{H(\omega_1)} \simeq -\phi_{H(\omega_2)}$ and vice-versa. As shown by (10), the differences between the components at the positive

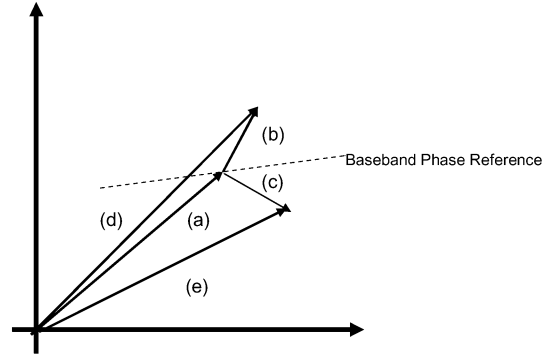


Fig. 4. Phasor addition of first and second slice components depicting phase reference of baseband components producing asymmetries in IM3 phase and magnitude. Components of the IM3 response are: (a) odd-ordered output from first slice, (b) upper (lower) baseband IM contribution from second slice, (c) lower (upper) baseband IM contribution from second slice, (d) total upper (lower) IM3 response from sum of slice outputs, and (e) total lower (upper) IM3 response from sum of slice outputs.

and negative baseband frequencies are the phase terms ϕ_L and ϕ_{k_n} . Assuming that $L(s)$ is a real network (such as the dc-bias network) forces $\phi_{L(\omega_1 - \omega_2)} = -\phi_{L(\omega_2 - \omega_1)}$. Combined with ϕ_{k_n} , these two terms result in a complex conjugate phase response between the positive and negative baseband frequencies.

Now the output of the ideal mixer at the upper IM3 (IM3H) and IM3L products are, respectively,

$$z_{2,\omega_{\text{IM3H}}}(t) = \sum_{n=2}^N \sum_{l=0}^{\frac{n-2}{2}} \frac{|k_n|}{2^{n-1}} \binom{n}{l, \frac{n}{2} - l, \frac{n-2}{2} - l, l+1} \times A_{\omega_2}^{2l+2} A_{\omega_1}^{n-2l-1} |H(\omega)|^n \times \cos(\omega_{\text{IM3H}}t + 2\phi_2 - \phi_1 + \phi_{L(\omega_{\text{BBH}})} + \phi_{k_n}) \quad (11a)$$

and

$$z_{2,\omega_{\text{IM3L}}}(t) = \sum_{n=2}^N \sum_{l=0}^{\frac{n-2}{2}} \frac{|k_n|}{2^{n-1}} \binom{n}{\frac{n}{2} - l, l, l+1, \frac{n-2}{2} - l} \times A_{\omega_1}^{2l+2} A_{\omega_2}^{n-2l-1} |H(\omega)|^n \times \cos(\omega_{\text{IM3L}}t + 2\phi_1 - \phi_2 + \phi_{L(\omega_{\text{BBL}})} - \phi_{k_n}). \quad (11b)$$

At this point, adding the effect of the output network $K(s)$ is trivial.

The actual phase reference about which the baseband components are complex conjugates is evident from the results of measurement. The phasor plot in Fig. 4 shows how the symmetric magnitudes of the upper and lower baseband terms can create IM3 responses that have both amplitude and phase asymmetry. A special case of the combination between the odd-order and baseband slice is when these share a common phase reference. In this situation, only phase asymmetries arise, and the IM3 terms rotate in a complex conjugate manner as a function of the ϕ_{k_n} 's, which changes the overall phase of the IM3 products as the higher order terms dominate at higher input power levels.

C. Model Parameter Extraction

Here, we describe the procedure for extracting the components of the two-slice model of Fig. 3. The process for estimating the frequency response of the macrolevel memory blocks $H(s)$ and $K(s)$ was developed in [8], and a similar series of steps can be used to determine the frequency response of $L(s)$ as a function of stimulus tone separation. The major task to be described here is extraction of the two sets of complex polynomial coefficients a_i and k_i .

The approach to the sequence of parameter estimation for the various slices is performed in order of the contribution to the nonlinear response. The odd-ordered polynomial in the first slice dominates this response so this slice is determined first. Extraction of the coefficients of the memoryless polynomial $f(\cdot)$ follows the traditional AM–AM AM–PM approach of fitting the single-tone response with the optimum fit in the least squares sense. With this slice determined, the next step is to fit the difference between the first slice estimate of the IM3 products and the measured two-tone data with the even-order baseband polynomial. The difference is given by

$$V_{\text{IM3,meas}} - V_{\text{IM3,est}} = V_{\text{IM3,diff}}. \quad (12)$$

There are actually two differences, one for each of the IM3 products. The value that is fitted is the average difference between the measured IM3 products and the estimated first-slice component with one of the IM3 differences applied as a complex conjugate. Once the coefficients are generated, the baseband contribution to IM3 are computed with (10) and then summed with the first slice output to yield the total model response.

Error functions based on the difference between the estimate and measured complex IM3 response are used to determine the polynomial order used in the fitting process. The order is adjusted to achieve the minimum error for each slice with respect to the IM3 tones even in the case of the first slice, which only uses single-tone information to compute the slice parameters.

IV. RESULTS

Multislice behavioral models were developed from IM3 vector measurements using the extraction procedure for three different power amplifiers. The amplifiers consisted of a 5-W multistage GaAs/silicon MESFET amplifier (ZHL-5W-1, Mini-Circuits, Brooklyn, NY), a high-linearity 10-W instrumentation MOSFET amplifier (1000W10, Amplifier Research, Souderton, PA), and an SiGe HBT Darlington driver amplifier mounted on an evaluation board (HMC479ST89, Hittite, Chelmsford, MA). The data collection process consisted of using the measurement system in Fig. 1 to measure the single-tone AM–AM AM–PM responses, and the amplitude and phase of the IM3 products during two-tone testing. For this study, the response of the amplifiers were measured at 450 MHz for f_1 and with a frequency separation of 10 kHz. The input power levels were swept from the small-signal region of each amplifier to the saturation point or to the maximum level recommended by the manufacturer if lower. The power at which the phase reference point was chosen depended on the amplifier under test and corresponded to the small-signal input region of the stimulus.

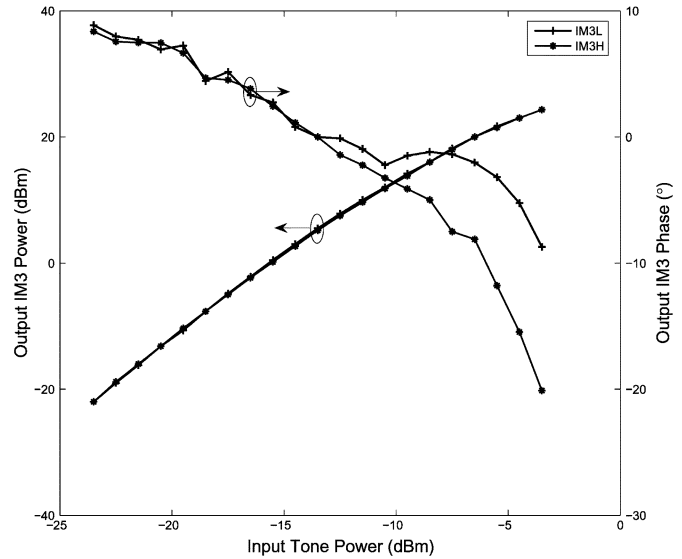


Fig. 5. Measured magnitude and phase of the IM3 products for the Mini-Circuits 5-W amplifier.

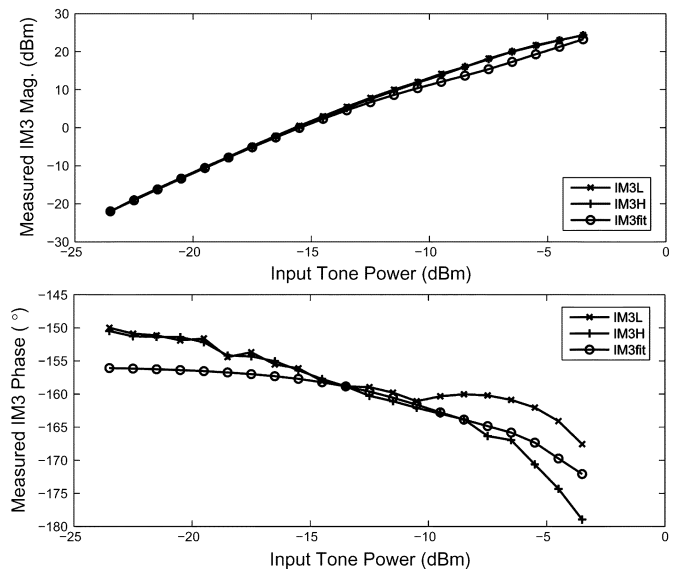


Fig. 6. Measured and estimated magnitude and phase of Mini-Circuits amplifier IM3 products using a single-slice model.

A. MESFET Amplifier

Measurements from a two-tone test of the GaAs MESFET amplifier are shown in Fig. 5 where the amplitude and phase measurement of the IM3 products are plotted. The amplifier does not exhibit amplitude asymmetry of the IM3H and IM3L, but there is phase asymmetry. The asymmetry becomes apparent as the input power level increases above the small-signal regime where gain compression begins to occur. The first step in the model extraction procedure was to determine the odd-ordered polynomial coefficients from the AM–AM AM–PM data. The result of this step is shown in Fig. 6 for a complex polynomial of order 15. As expected, the resulting fit cannot track the asymmetry in the IM3 phase, however, the IM3 magnitude fit also fails to track the measured response. The error in the single-slice magnitude fit occurs at the same input power level as appearance

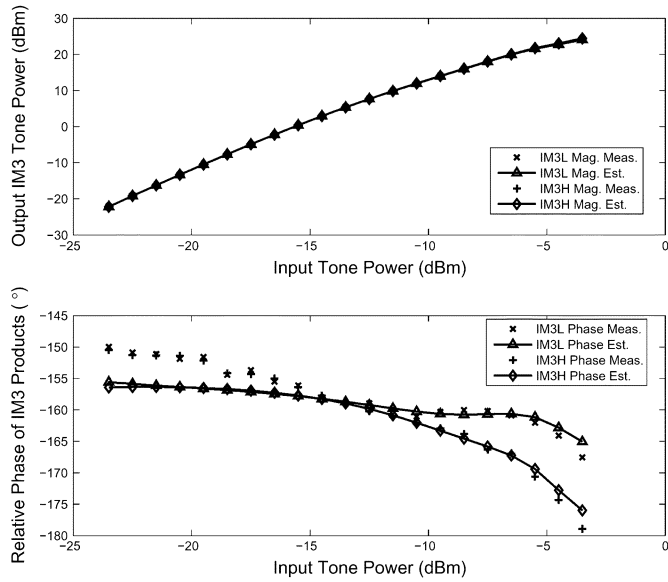


Fig. 7. Measured and estimated magnitude and phase of Mini-Circuits amplifier IM3 products using a two-slice model.

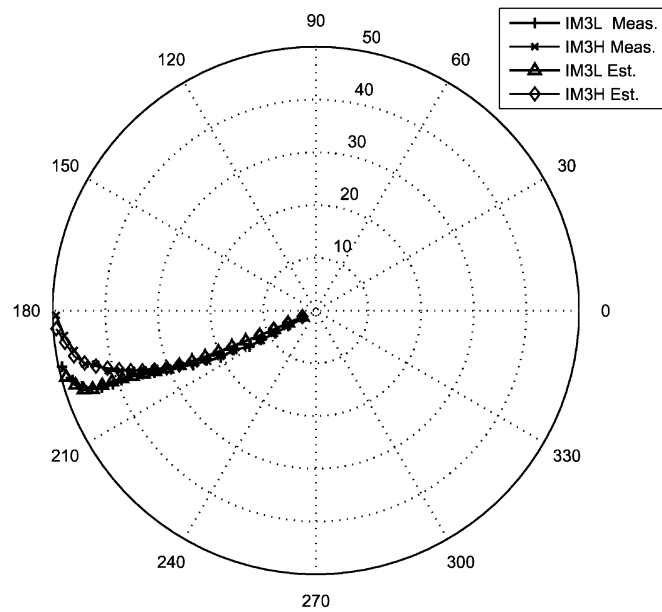


Fig. 8. Polar form of the fit to the Mini-Circuits amplifier IM3 data with the magnitude in decibels (magnitudes offset such that they are nonnegative).

of the asymmetric behavior in the phase of the IM3H and IM3L products. This is strong evidence that the upconversion of baseband effects from an even-order nonlinearity are becoming important. The fit of the odd-ordered model reinforces this hypothesis since the phase component of the fit roughly splits the difference in phase between the two IM3 products. This corresponds to the case in Fig. 4 where the baseband component has the same phase reference as the strictly odd-ordered components.

With the first slice of the multislice model extracted, the next step in the extraction procedure was to determine the even-order coefficients (in this case, up to eighth order) for the nonlinearity that produces the baseband terms. The result of this step and the summation in a phasor sense of the second slice with the first slice is shown in Fig. 7. The resulting fit of the two-slice model

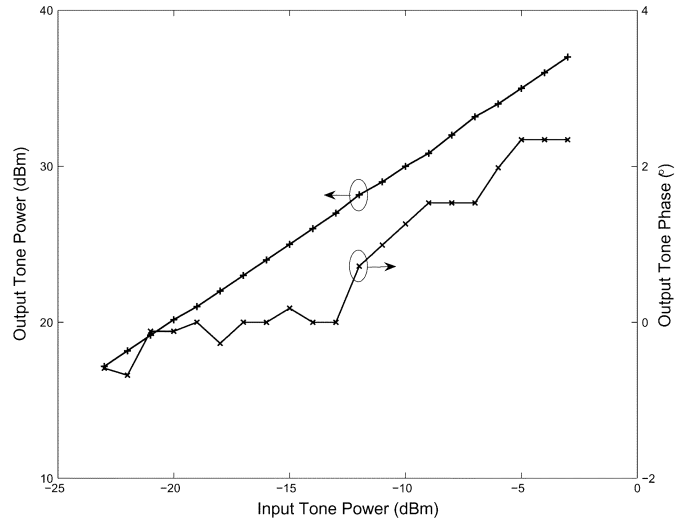


Fig. 9. Measured AM-AM AM-PM of the 10-W AR amplifier.

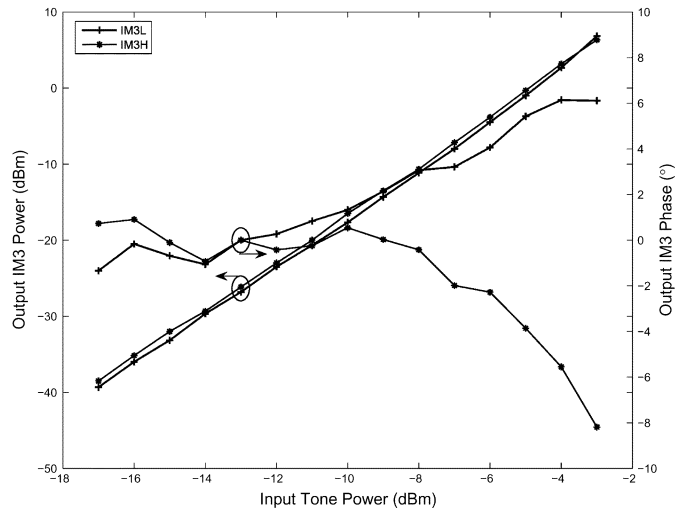


Fig. 10. Measured magnitude and phase of the IM3 products for the AR amplifier.

was < 0.5 dB for the magnitude of the IM3 products and the phase estimation was $< 3^\circ$ for the majority of the input power sweep, except for the small-signal region. It is more illustrative to plot the measured and modeled IM3 responses on a polar plot, as shown in Fig. 8.

B. MOSFET Instrumentation Amplifier

The instrumentation MOSFET amplifier was expected to have a very weak nonlinear response since its purpose is to provide laboratory-grade amplification without distortion. The single-tone data (Fig. 9) does not indicate any onset of compression for an input power of up to -3 dBm. However, the phase of the output tone does begin to exhibit small AM-PM distortion as the input power is increased. The weak nonlinear response is also seen in the two-tone IM3 measurements (Fig. 10). Here, the IM3 tones are strictly 3:1 in slope with the asymmetry consisting of a systematic type error. For this data, the IM3 phase data is informative about the source of the nonlinearities contributing to the IM3 products. The phase response of the

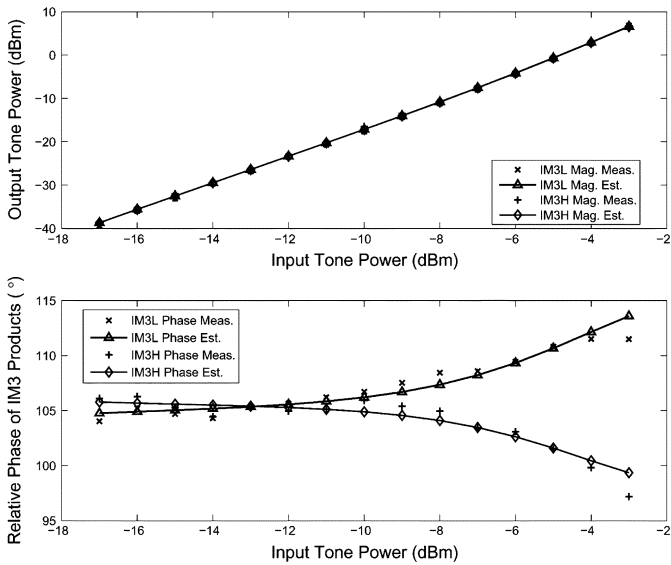


Fig. 11. Measured and modeled magnitude and phase of the IM3 products of the MOSFET instrumentation amplifier.

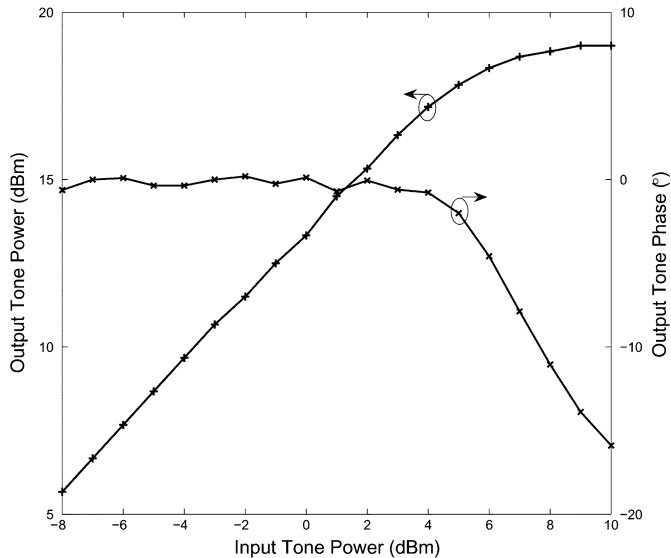


Fig. 12. Measured AM-AM and AM-PM of the Darlington HBT amplifier.

IM3H and IM3L products clearly has a complex conjugate relationship over the entire power range suggesting that the baseband upconversion term generates the entire IM3 response. This hypothesis was reinforced by the relatively low order of the odd-ordered nonlinearity required to minimize the error functions presented in Section III, i.e., that of $N_{s1} = 5$ and $N_{s2} = 8$, for the first and second slices, respectively.

Applying the fitting procedure for the two-slice model yielded a very good fit to the IM3 data (Fig. 11). Here, the error in the IM3 amplitude was <0.7 dB and the maximum error for the IM3 phase was 2.17° with an average phase error of 0.57° for the IM3L and 0.59° for IM3H. This phase error lies below the uncertainty of the phase measurement itself.

C. Darlington HBT Amplifier

The Darlington HBT amplifier investigated exhibited the most complex nonlinear response of all of the amplifiers. The

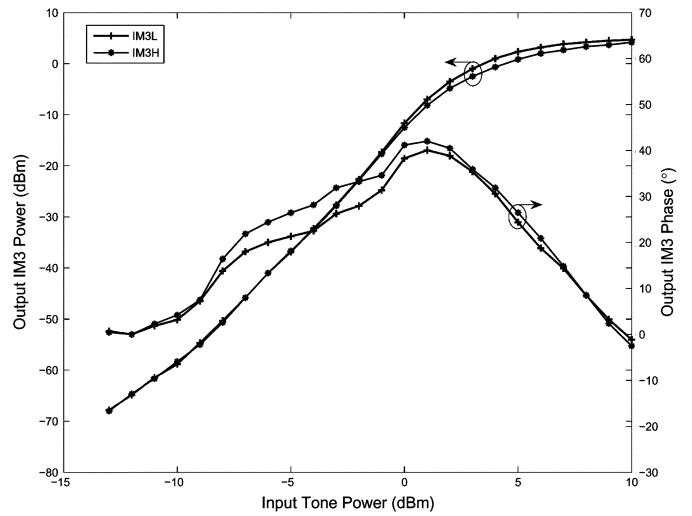


Fig. 13. Measured magnitude and phase of the IM3 products for the Darlington HBT amplifier.

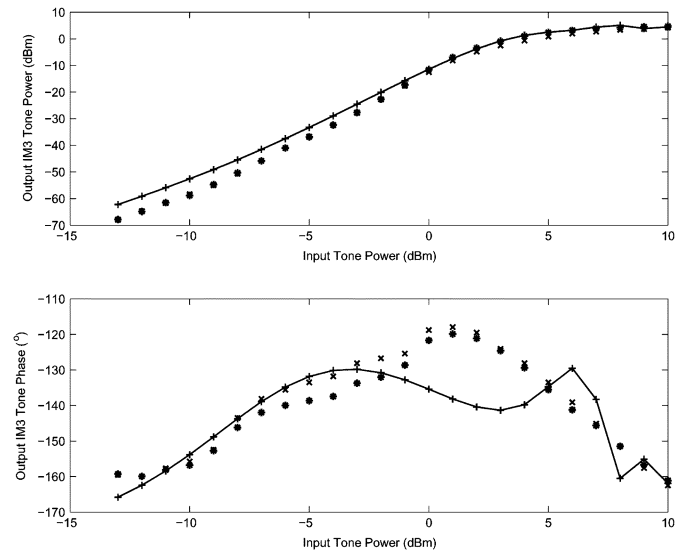


Fig. 14. Measured and estimated magnitude and phase of Hittite amplifier IM3 products using nonlinear optimization fitting technique to extract the one-slice model (*: IM3L measured, \times : IM3H measured, +: nonlinear optimization fit to both data sets).

AM-AM and AM-PM measurements showed a typical response of a constant phase insertion for small-signal input levels with a change in phase as the gain became compressed and neared the saturation power level (Fig. 12). In contrast, the response of both the magnitude and phase of the IM3 products deviated considerably from the kind of response that could be captured by a polynomial (see Fig. 13).

The behavior of the IM3 phase of this amplifier led to difficulties in applying the fitting procedure of the two-slice model, as outlined previously. With the other amplifiers considered, it was possible to initially fit the first slice and then fit the second. Here, it was necessary to fit both slices simultaneously.

The nonlinear fitting procedure used the Levenberg-Marquardt search method. Both the measured one- and two-tone data sets were supplied to the routine to search for the appropriate solution over the problem space. This approach did

produce the best result in terms of minimum squared error of the IM3 fit; however, there was still considerable error in the IM3 phase estimation and overestimation of the IM3 magnitude by as much as 6 dB (Fig. 14).

V. CONCLUSION

A scheme with 90-dB dynamic range and a maximum phase uncertainty of 2° has been presented for measuring the amplitude and phase of intermodulation products in a two-tone test. The measurement procedure was coupled with the introduction of a two-slice behavioral model and a suitable extraction procedure. The behavioral model is an architecture for capturing higher order nonlinearities that cannot be captured in a single-tone test and many possible conventional behavioral models could be used for each slice. Here, a Weiner-Hammerstein LNL block model was used with complex polynomials describing the nonlinearities. The model was used with three different types of amplifiers, and it was shown that the characteristics of the amplifiers in one- and two-tone tests could be captured. Most importantly, it was seen that amplitude and phase asymmetries in the IM3 response of a two-tone test could be adequately be captured. The two-slice model is an extension of conventional AM-AM and AM-PM models so the existing modeling and measurement infrastructure can be utilized.

REFERENCES

- [1] J. C. Pedro, N. B. Carvalho, and P. Lavrador, "Modeling nonlinear behavior of bandpass memoryless and dynamic systems," in *IEEE MTT-S Int. Microw. Symp. Dig.*, Jun. 2003, vol. 3, pp. 2133–2136.
- [2] K. G. Gard, H. M. Gutierrez, and M. B. Steer, "Characterization of spectral regrowth in microwave amplifiers based on the nonlinear transformation of a complex Gaussian process," *IEEE Trans. Microw. Theory Tech.*, vol. 47, no. 7, pp. 1059–1069, Jul. 1999.
- [3] K. Gharaibeh and M. Steer, "Modeling distortion in multichannel communication systems," *IEEE Trans. Microw. Theory Tech.*, vol. 53, no. 5, pp. 1682–1692, May 2005.
- [4] H. Ku and J. S. Kenney, "Behavioral modeling of nonlinear RF power amplifiers considering memory effects," *IEEE Trans. Microw. Theory Tech.*, vol. 51, no. 5, pp. 2495–2504, May 2005.
- [5] A. Soury, E. Ngoya, and J. Rousset, "Behavioral modeling of RF and microwave circuit blocks for hierarchical simulation of modern transceivers," in *IEEE MTT-S Int. Microw. Symp. Dig.*, Jun. 2005, pp. 975–978.
- [6] N. B. de Carvalho and J. C. Pedro, "A comprehensive explanation of distortion sideband asymmetries," *IEEE Trans. Microw. Theory Tech.*, vol. 50, no. 9, pp. 2090–2101, Sep. 2002.
- [7] D. J. Williams, J. Leckey, and P. J. Tasker, "A study of the effect of envelope impedance on intermodulation symmetry using a two-tone time domain measurement system," in *IEEE MTT-S Int. Microw. Symp. Dig.*, Jun. 2002, vol. 3, pp. 1841–1844.
- [8] A. Walker, M. Steer, K. Gard, and K. Gharaibeh, "Multi-slice behavioral model of RF systems and devices," in *Radio Wireless Conf. Dig.*, Sep. 2004, pp. 71–74.
- [9] U. Lott, "A method for measuring magnitude and phase of harmonics generated in nonlinear microwave two-ports," in *IEEE MTT-S Int. Microw. Symp. Dig.*, May 1998, vol. 1, pp. 225–228.
- [10] A. Walker, M. Steer, and K. Gard, "Simple, broadband relative phase measurement of intermodulation products," in *Proc. 65th ARFTG Conf.*, Jun. 2005, pp. 123–127.
- [11] A. Walker, M. B. Steer, and K. Gard, "Capturing the phase asymmetry of distortion in a nonlinear RF system using a multi-slice behavioral model," *IEEE Microw. Wireless Compon. Lett.*, to be published.

- [12] N. Suematsu, T. Shigematsu, Y. Iyama, and O. Ishida, "Transfer characteristic of IM3 relative phase for a GaAs FET amplifier," in *IEEE MTT-S Int. Microw. Symp. Dig.*, Jun. 1997, vol. 2, pp. 901–904.
- [13] Y. Yang, J. Yi, J. Nam, B. Kim, and M. Park, "Measurement of two-tone transfer characteristics of high-power amplifiers," *IEEE Trans. Microw. Theory Tech.*, vol. 49, no. 3, pp. 568–571, Mar. 2001.
- [14] *Calibration Guide Agilent Technologies 8560 E-Series and EC-Series Spectrum Analyzers*. Palo Alto, CA: Agilent Technol., 2002, vol. I and II.
- [15] "Large signal network analyzer technology preliminary product overview," Maury Microw. Corporation, Ontario, CA, May 2003.
- [16] "Minutes of the 4th ARFTG NVNA Users' Forum," 4th ARFTG NVNA Users' Forum, Jun. 2004.
- [17] J. H. K. Vuolevi, T. Rahkonen, and J. P. A. Manninen, "Measurement technique for characterizing memory effects in RF power amplifiers," *IEEE Trans. Microw. Theory Tech.*, vol. 49, no. 8, pp. 1383–1389, Aug. 2001.
- [18] P. Heymann, R. Doerner, and M. Rudolph, "Multiharmonic generators for relative phase calibration of nonlinear network analyzers," *IEEE Trans. Instrum. Meas.*, vol. 50, no. 1, pp. 129–134, Feb. 2001.
- [19] C. Crespo-Cadenas, J. Reina-Tosina, and M. J. Madero-Ayora, "Phase characterization of two-tone intermodulation distortion," in *IEEE MTT-S Int. Microw. Symp. Dig.*, Jun. 2005, 4 pages.
- [20] J. C. Pedro, J. P. Martins, and P. M. Cabral, "New method for phase characterization of nonlinear distortion products," in *IEEE MTT-S Int. Microw. Symp. Dig.*, Jun. 2005, pp. 971–974.
- [21] D. D. Weiner and J. F. Spina, *Sinusoidal Analysis and Modeling of Weakly Nonlinear Circuits*. New York: Van Nostrand, 1980.



Aaron Walker (S'95–M'99) received the B.S. degree in nuclear engineering from Kansas State University, Manhattan, in 1997, and the M.S. and Ph.D. degrees in electrical engineering from North Carolina State University, Raleigh, in 1999 and 2006, respectively.

From 1999 to 2002 he was an Application Specific Integrated Circuit (ASIC) Design Engineer with Atmel and Zaiq Technologies. He is currently the President of Vadum Inc., Raleigh, NC. His interests include nonlinear system characterization and

identification, remote sensing, and behavioral modeling.



Michael Steer (S'76–M'82–SM'90–F'99) received the B.E. and Ph.D. degrees in electrical engineering from the University of Queensland, Brisbane, Australia, in 1976 and 1983, respectively.

He is currently the Lampe Family Distinguished Professor of Electrical and Computer Engineering, North Carolina State University, Raleigh. In 1999 and 2000, he was a Professor with the School of Electronic and Electrical Engineering, The University of Leeds, where he held the Chair in microwave and millimeter-wave electronics. He was also Director of the Institute of Microwaves and Photonics, The University of Leeds. He has authored over 300 publications on topics related to RF, microwave and millimeter-wave systems, high-speed digital design, and RF and microwave design methodology and circuit simulation. He coauthored *Foundations of Interconnect and Microstrip Design* (Wiley, 2000).

Prof. Steer is active in the IEEE Microwave Theory and Techniques Society (IEEE MTT-S). In 1997, he was secretary of the IEEE MTT-S. From 1998 to 2000, he was an elected member of its Administrative Committee. He is the Editor-in-Chief of the IEEE TRANSACTIONS ON MICROWAVE THEORY AND TECHNIQUES (2003–2006). He was a 1987 Presidential Young Investigator (USA). In 1994 and 1996, he was the recipient of the Bronze Medallion presented by the Army Research Office for "Outstanding Scientific Accomplishment." He was also the recipient of the 2003 Alcoa Foundation Distinguished Research Award presented by North Carolina State University.



Kevin G. Gard (S'92–M'95) received the B.S. and M.S. degrees in electrical engineering from North Carolina State University, Raleigh, in 1994 and 1995, respectively, and the Ph.D. degree in electrical engineering from the University of California at San Diego, in 2003.

He is currently the William J. Pratt Assistant Professor with the Electrical and Computer Engineering Department, North Carolina State University. From 1996 to 2003, he was with Qualcomm Inc., San Diego, CA, where he was a Staff Engineer and

Manager responsible for the design and development of RF integrated circuits (RFICs) for code-division multiple-access (CDMA) wireless products. He has designed SiGe BiCMOS, Si BiCMOS, and GaAs metal–semiconductor field-effect transistor (MESFET) integrated circuits for cellular and personal communication systems (PCSs) CDMA, wideband code-division multiple-access (WCDMA), and AMPS transmitter applications. His research interests are in the areas of integrated circuit design for wireless applications and analysis and modeling of nonlinear microwave circuits with digitally modulated signals.